

Supramolecular architecture, crystal structure and transport properties of the prototypal oxobenzene-bridged bisdithiazolyl radical conductor†

Cite this: *Chem. Commun.*, 2014, 50, 785

Received 2nd September 2013,
Accepted 25th September 2013

DOI: 10.1039/c3cc46686h

www.rsc.org/chemcomm

Joanne W. L. Wong,^a Aaron Mailman,^a Stephen M. Winter,^a Craig M. Robertson,^b Rebecca J. Holmberg,^c Muralee Murugesu,^c Paul A. Dube^d and Richard T. Oakley*^a

Supramolecular CH $\cdots\pi$ interactions cause a ruffling of the otherwise coplanar ribbon-like arrays of radicals in the structure of the oxobenzene-bridged bisdithiazolyl **1a. The material displays a conductivity $\sigma(300\text{ K}) = 6 \times 10^{-3}\text{ S cm}^{-1}$ ($E_{\text{act}} = 0.16\text{ eV}$) and orders antiferromagnetically below 4 K. At applied fields above 1 kOe the material displays metamagnetic behavior.**

Heterocyclic thiazyl radicals have been widely studied as building blocks for magnetic and conductive materials, in part because the presence of sulfur (a heavy heteroatom) enhances intermolecular magnetic and electronic interactions.¹ Within this context oxobenzene-bridged bisdithiazolyls **1** represent a new and potentially powerful building block for the design of molecule-based conductors.² Their highly delocalized spin distributions help suppress dimerization and, at the same time, decrease the Mott-Hubbard onsite Coulomb barrier to charge transfer U .³ From a structural perspective, the crystal packing of these radicals is strongly influenced by intermolecular S \cdots O' and S \cdots N' contacts, which serve as supramolecular synthons⁴ to generate ribbon-like arrays, as in Chart 1.

The overlay of these molecular ribbons gives rise to a variety of patterns, including head-over-tail π -stacks **A** (**1d,e**),^{2c,d} slipped π -stacks **B** (**1c**),^{2b} and brick wall motifs **C** (**1b**).^{2a} While the bandwidth W generated by these packing patterns is insufficient to overcome U , these materials nonetheless display high conductivity, with $\sigma(300\text{ K})$ in the range of 10^{-4} to 10^{-2} S cm^{-1} , and with thermal activation energies $E_{\text{act}} = 0.20$ to 0.10 eV . In the case of **1b**, metallization has been achieved by compression to just 3 GPa.^{2a} Here we report the preparation and structural characterization of the prototypal derivative **1a**. Despite its small size, the basal proton plays a major role in determining solid state structure and transport properties.



Scheme 1

To prepare the desired framework, while at the same time avoiding chlorination of the basal carbon,^{2b} we started with 2,6-diaminoanisole **2**,⁵ which was converted sequentially into the 3,5-bis(thiocyanato) **3** and

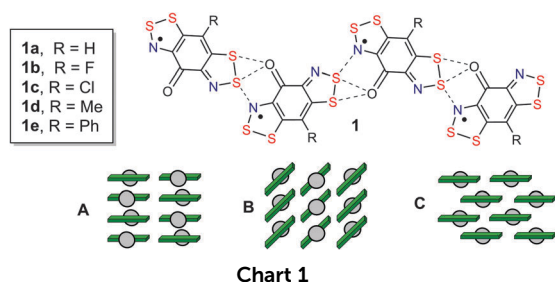


Chart 1

^a Department of Chemistry, University of Waterloo, Waterloo, Ontario, N2L 3G1, Canada. E-mail: oakley@uwaterloo.ca

^b Department of Chemistry, University of Liverpool, Liverpool L69 7ZD, UK

^c Department of Chemistry, University of Ottawa, Ottawa, Ontario, K1N 6N5, Canada

^d Brockhouse Institute for Materials Research, McMaster University, Hamilton, Ontario L8S 4M1, Canada

† Electronic supplementary information (ESI) available: Details of synthetic, spectroscopic and magnetic work. CCDC 957990. For ESI and crystallographic data in CIF or other electronic format see DOI: 10.1039/c3cc46686h

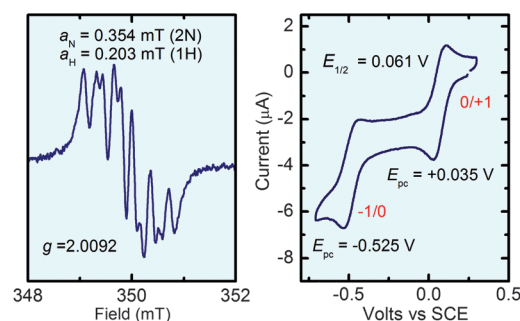


Fig. 1 (a) X-band EPR spectrum of **1a** in CS₂. (b) CV scan of [**1a**][ONf] with Pt electrodes, 0.1 M *n*-Bu₄NPF₆ electrolyte, scan rate 100 mV s⁻¹.

3,5-dithiol **4** (Scheme 1). Subsequent cyclocondensation of **4** with thionyl chloride yielded the desired salt [**1a**][Cl] without any contamination with [**1c**][Cl]. Metathesis with silver nonaflate AgONf in MeCN afforded, after solvent removal, metallic green crystals of [**1a**][ONf]. Reduction of the latter with octamethylferrocene (OMFc) in MeCN yielded metallic bronze microcrystals of **1a**.

The electronic structure of the radical in solution has been probed by EPR spectroscopy and cyclic voltammetry (Fig. 1). The X-band EPR spectrum of **1a** in CS₂ is consistent with a highly delocalized spin distribution, consisting of a doublet of pentets arising from hyperfine coupling to two equivalent ¹⁴N nuclei with $a_N = 0.354$ mT, and to the basal proton with $a_H = 0.203$ mT. Cyclic voltammetry on a solution of [**1a**][ONf] in MeCN (Fig. 1b) indicates a reversible +1/0 couple with $E_{1/2} = +0.061$ V vs. SCE and a second irreversible reduction, corresponding to the -1/0 couple, with a cathodic peak potential $E_{pc} = -0.525$ V vs. SCE. From the difference in the E_{pc} for the two couples we estimate a cell potential $E_{cell} = 0.56$ V, to date the lowest observed for a radical of this type, which augurs well for a low onsite Coulomb potential U .⁶

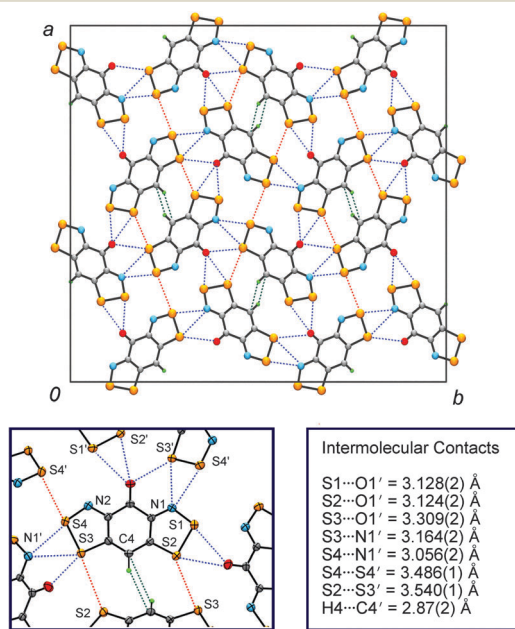


Fig. 2 Unit cell of **1a**, with ribbon-like arrays of radicals following the *d*-glide planes. Intra-ribbon S...O' and S...N' connectors are in blue, CH...C' contacts along the 2₁ axes in green, and inter-ribbon S...S' contacts in red. The ORTEP drawing and table below specify distances.

X-ray diffraction analysis of microcrystals of **1a** required synchrotron radiation methods. The crystal structure belongs to the polar orthorhombic space group *Fdd2* and consists of slipped π -stacks of evenly spaced radicals running parallel to the *c*-axis. The unit cell drawing in Fig. 2 provides a view of the 16 symmetry related radicals ($Z = 16$), and illustrates the ribbon-like motifs generated by the *d*-glide planes that run perpendicular to the *x* and *y* directions. Also shown is the network of intermolecular S...O', S...N', S...S' and CH...C' contacts (all inside the respective van der Waals separation).⁷

While the projection shown in Fig. 2 suggests architectural similarities with other radicals of this type, there are some important

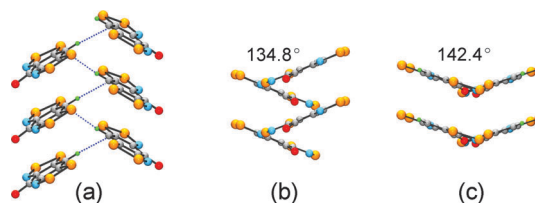


Fig. 3 (a) Tilted-T CH...C' contacts along the 2₁ axis. End-on views of molecular ribbons running perpendicular to the (b) *x*- and (c) *y*-directions, with dihedral angles showing extent of ruffling.

differences, the most notable arising from the presence of edge-to-face or tilted-T CH... π interactions⁸ along the 2₁ axes (Fig. 3). This local herringbone arrangement forces radicals out of coplanarity, and causes a ruffling of the otherwise planar ribbon-like arrays along *x* and *y*, as indicated by the dihedral angles of 142.4° and 134.8°. The resulting slipped π -stacks, with a plate-to-plate separation of 3.47 Å, are inclined at an angle of 29.8° to the *c*-axis.

DC magnetic susceptibility (χ) measurements on **1a** have been performed over the temperature range $T = 2$ –300 K. Initial field-cooled experiments (Fig. 4a) at a field of $H = 1$ kOe suggest Curie-Weiss behavior with strong local ferromagnetic interactions; a fit to the data from 30–300 K affords a *C*-constant of 0.364 emu mol⁻¹ and a large θ value of +15.6 K. Below 10 K, there is a rapid increase in both χ and χT , the latter reaching a maximum value near 9.0 emu K mol⁻¹ near 5.0 K.

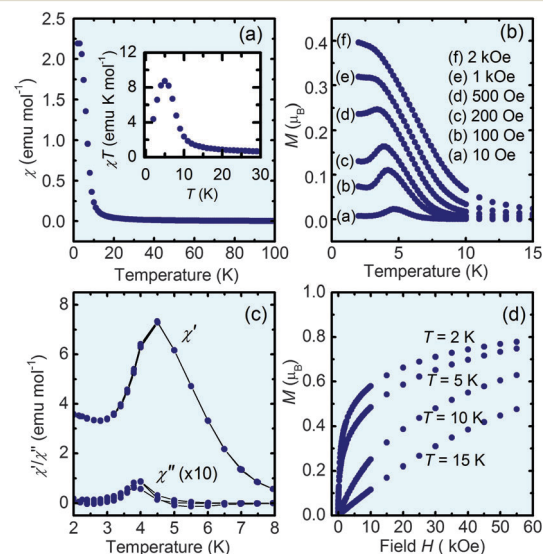


Fig. 4 (a) Field-cooled DC susceptibility χ of **1a** from $T = 2$ –100 K with $H = 1$ kOe; insert shows χT vs. T (from 2–30 K). (b) Magnetization (M) vs. T plots at different fields (H). (c) Overlays of AC susceptibility χ' and χ'' ($\times 10$) vs. T plots at 10, 100 and 1000 Hz. (d) Magnetization (M) vs. field (H) plots at different temperatures.

At magnetic fields lower than 1 kOe, the susceptibility no longer increases continuously with decreasing temperature. Instead, a maximum emerges in the $\chi(T)$ plot near 4 K, indicative of the onset of antiferromagnetic interactions below this temperature. The results of subsequent $M(T)$ measurements (Fig. 4b) over a range of magnetic fields H are consistent with metamagnetic behavior,⁹ that is, a system which, at low field, possesses an AFM ordered ground state, but which experiences field induced re-alignment at higher applied fields, so as to produce an FM ordered state. From the position of the

maximum in the low field $M(T)$ plots, the ordering temperature T_N for the AFM state can be estimated near 4 K. The critical field H_c required to invert the ordering can be approximated in terms of the turnover point in the $M(T)$ plots, where the AFM maximum at 4 K in the $M(T)$ curves disappears; on this basis we estimate $H_c \sim 1$ kOe.

AC susceptibility measurements (Fig. 4c) support this interpretation and provide a more precise measure of the ordering temperature. At all cycling frequencies from 0.1 Hz to 1 kHz, the in-phase component χ' shows a clear, frequency independent maximum at 4.5 K, which corresponds closely to the value obtained from DC cooling curve experiments. The response of the out-of-phase component χ'' is much weaker, as would be expected for a low dimensional system.

The field dependence of the phase transition can be seen more clearly in isothermal magnetization measurements. As shown in Fig. 4d, typical paramagnetic behavior is observed above 15 K, but below this temperature the $M(H)$ curves rise rapidly, indeed far more quickly than related radicals that undergo field induced FM ordering.¹⁰ Also in contrast to other radical-based metamagnets, and despite the low field required to induce magnetization reversal, the magnetization is extremely slow to reach the full FM saturation value $M_{\text{sat}} = 1 \mu_B$ expected for a $S = \frac{1}{2}$ system with a nominal $g = 2$. At $T = 2$ K, the value of $M(H)$ is still rising at $H = 50$ kOe, the limit of our experiments, but has only reached $0.8 \mu_B$, or 80% of the full saturation value. This result is perhaps not too surprising, when considered in conjunction with the low value of $T_N/\theta = 0.3$ and a positive Weiss constant in a material that displays AFM ordering. Given the complexity of the crystal structure, and the consequently large number of magnetic exchange interactions, low dimensional and/or frustrated character to the magnetic response is likely, and in such circumstances magnetization plateaus are commonly observed.¹¹

We reported earlier the results of ambient pressure, variable temperature conductivity (σ) measurements on the derivatives **1b–1e**.² Similar measurements, using the four-probe method on cold-pressed pellets, have now been performed on **1a**. Results for the entire set are illustrated in Fig. 5, in the form of log plots of σ against $1/T$. As may be seen, the conductivity of **1a** $\sigma(300 \text{ K}) = 6 \times 10^{-3} \text{ S cm}^{-1}$, places it near the top of the pack, but its activation energy, $E_{\text{act}} = 0.16 \text{ eV}$, is a little higher than the average.

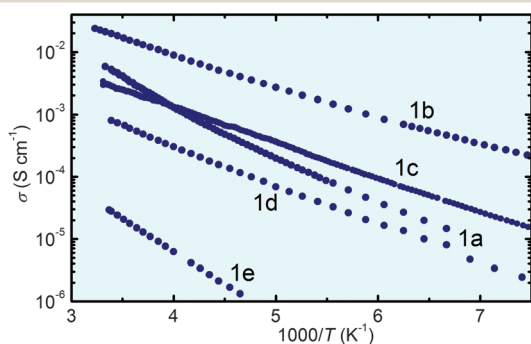


Fig. 5 Plots of $\log \sigma$ versus $1/T$ for radicals **1a–e**; data for **1c** correspond to the MeCN adduct. Data for **1b–1e** are from ref. 2.

Strong lateral $F \cdots S'$ contacts in **1b**, in combination with $S \cdots O'$ and $S \cdots N'$ interactions, link ribbons of radicals into rigorously coplanar sheets of radicals, which gives rise to a brick wall

architecture (Chart 1C) with a well developed 2D electronic structure.^{2a} By contrast, the role of the $CH \cdots \pi$ supramolecular synthons in **1a** is to disrupt the coplanarity of radicals, to ruffle the molecular ribbon motif and produce a slipped π -stack architecture with a more 1D electronic structure. As a result the performance of **1a**, in terms of $\sigma(300 \text{ K})$ and E_{act} , is marginally lower than that of **1b**. The material is nonetheless very close to the Mott insulator/metal transition, and its ruffled ribbon structure is likely more compressible¹² than the layered sheets of **1b**, in which case its pressure induced metallization may be a relatively facile process.

We thank the Natural Sciences and Engineering Research Council of Canada for financial support.

Notes and references

‡ Crystal data at 296.15 K for **1a**: $C_6H_4N_2S_4$ $M = 245.33$, orthorhombic, $a = 27.876(3) \text{ \AA}$, $b = 31.252(4) \text{ \AA}$, $c = 4.0004(5) \text{ \AA}$, $V = 3485.2(7) \text{ \AA}^3$, space group $Fdd2$ (#42), $Z = 16$, $D_{\text{calcd}} = 1.870 \text{ g cm}^{-3}$, $\mu = 1.042 \text{ mm}^{-1}$, $\text{flack} = 0.06(8)$; 122 parameters were refined using 1873 unique reflections ($R_{\text{int}} = 0.0235$) to give $R = 0.0235$ and $R_w = 0.524$ (observed data).

- (a) J. M. Rawson, A. Alberola and A. Whalley, *J. Mater. Chem.*, 2006, **16**, 2560; (b) R. G. Hicks, in *Stable Radicals: Fundamentals and Applied Aspects of Odd-Electron Compounds*, ed. R. G. Hicks, John Wiley & Sons, Ltd., Wiltshire, 2010, p. 317; (c) I. Ratera and J. Veciana, *Chem. Soc. Rev.*, 2012, **41**, 303; (d) R. C. Haddon, *ChemPhysChem*, 2012, **13**, 3581; (e) R. T. Boeré and T. L. Roemmele, *Comp. Inorg. Chem. II*, 2013, vol. 1, p. 375; (f) J. M. Rawson, J. J. Hayward, *Handbook of Chalcogen Chemistry: New Perspectives in Sulfur, Selenium and Tellurium*, 2013, vol. 2, p. 69; (g) A. W. Cordes, R. C. Haddon and R. T. Oakley, *Phosphorus, Sulfur Silicon Relat. Elem.*, 2004, **179**, 673; (h) K. E. Shuvaev and J. Passmore, *Coord. Chem. Rev.*, 2013, **257**, 1067; (i) K. E. Preuss, *Dalton Trans.*, 2007, 2357.
- (a) A. Mailman, S. M. Winter, X. Yu, C. M. Robertson, W. Yong, J. S. Tse, R. A. Secco, Z. Liu, P. A. Dube, J. A. K. Howard and R. T. Oakley, *J. Am. Chem. Soc.*, 2012, **134**, 9886; (b) X. Yu, A. Mailman, K. Lekin, A. Assoud, C. M. Robertson, B. C. Noll, C. F. Campana, J. A. K. Howard, P. A. Dube and R. T. Oakley, *J. Am. Chem. Soc.*, 2012, **134**, 2264; (c) X. Yu, A. Mailman, K. Lekin, A. Assoud, P. A. Dube and R. T. Oakley, *Cryst. Growth Des.*, 2012, **12**, 2485; (d) X. Yu, A. Mailman, P. A. Dube, A. Assoud and R. T. Oakley, *Chem. Commun.*, 2011, **47**, 4655.
- (a) N. F. Mott, *Proc. Phys. Soc., London, Sect. A*, 1949, **62**, 416; (b) J. Hubbard, *Proc. R. Soc. London Ser. A*, 1963, **276**, 238.
- G. R. Desiraju, *Angew. Chem., Int. Ed. Engl.*, 1995, **34**, 2311.
- (a) N. J. Clecak, S. Jose, R. J. Cox, L. Gatos, S. L. Solar, S. Jose and H. K. Wurster, *US Pat.*, 3489558, 1970; (b) A. Banerjee and I. N. Ngwendson, *US Pat.*, 20070179311 A1, 2007.
- R. T. Boeré and T. L. Roemmele, *Coord. Chem. Rev.*, 2000, **210**, 369.
- (a) A. J. Bondi, *J. Phys. Chem.*, 1964, **68**, 441; (b) I. Dance, *New J. Chem.*, 2003, **27**, 22.
- (a) S. Paliwal, S. Geib and C. S. Wilcox, *J. Am. Chem. Soc.*, 1994, **116**, 4491; (b) P. Hobza, H. L. Selzle and E. W. Schlag, *J. Am. Chem. Soc.*, 1994, **116**, 3500; (c) A. Gavezzotti and G. R. Desiraju, *Acta Crystallogr.*, 1988, **B44**, 427; (d) J. Bernstein, J. A. R. P. Sarma and A. Gavezzotti, *Chem. Phys. Lett.*, 1990, **174**, 361; (e) S. E. Wheeler and K. N. Houk, *Mol. Phys.*, 2009, **107**, 749.
- J. M. D. Coey, *Magnetism and Magnetic Materials*, Cambridge University Press, 2010.
- (a) S. M. Winter, K. Cvrkalj, P. A. Dube, C. M. Robertson, M. R. Probert, J. A. K. Howard and R. T. Oakley, *Chem. Commun.*, 2009, 7003; (b) W. Fujita, K. Takahashi and H. Kobayashi, *Cryst. Growth Des.*, 2011, **11**, 575; (c) H. Nagashima, S. Fujita, H. Inoue and N. Yoshioka, *Cryst. Growth Des.*, 2004, **4**, 19; (d) T. Ishida, K. Tomioka, T. Nogami, H. Yoshikawa, M. Yasui, F. Iwasaki, N. Takeda and M. Ishikawa, *Chem. Phys. Lett.*, 1995, **247**, 7.
- (a) G. Catilla, S. Chakravarty and V. J. Emery, *Phys. Rev. Lett.*, 1995, **75**, 1823; (b) M. Hase, H. Kuroe, K. Ozawa, O. Suzuki, H. Kitazawa, G. Kido and T. Sekine, *Phys. Rev. B: Condens. Matter Mater. Phys.*, 2004, **70**, 104426; (c) M. Kumar, S. E. Dutton, R. J. Cava and Z. G. Soos, *J. Phys.: Condens. Matter*, 2013, **25**, 136004.
- K. Lekin, A. A. Leitch, J. S. Tse, X. Bao, R. A. Secco, S. Desgreniers, Y. Ohishi and R. T. Oakley, *Cryst. Growth Des.*, 2012, **12**, 4676.